



ARTICLE

Acetyl-CoA synthetase 2 promotes diabetic renal tubular injury in mice by rewiring fatty acid metabolism through SIRT1/ChREBP pathway

Jian Lu¹, Xue-qi Li², Pei-pei Chen², Jia-xiu Zhang², Liang Li², Gui-hua Wang², Xiao-qi Liu³, Chun-ming Jiang¹✉ and Kun-ling Ma³✉

Diabetic nephropathy (DN) is characterized by chronic low-grade renal inflammatory responses, which greatly contribute to disease progression. Abnormal glucose metabolism disrupts renal lipid metabolism, leading to lipid accumulation, nephrotoxicity, and subsequent aseptic renal interstitial inflammation. In this study, we investigated the mechanisms underlying the renal inflammation in diabetes, driven by glucose-lipid metabolic rearrangement with a focus on the role of acetyl-CoA synthetase 2 (ACSS2) in lipid accumulation and renal tubular injury. Diabetic models were established in mice by the injection of streptozotocin and in human renal tubular epithelial HK-2 cells cultured under a high glucose (HG, 30 mmol/L) condition. We showed that the expression levels of ACSS2 were significantly increased in renal tubular epithelial cells (RTECs) from the diabetic mice and human diabetic kidney biopsy samples, and ACSS2 was co-localized with the pro-inflammatory cytokine IL-1 β in RTECs. Diabetic ACSS2-deficient mice exhibited reduced renal tubular injury and inflammatory responses. Similarly, ACSS2 knockdown or inhibition of ACSS2 by ACSS2i (10 μ mol/L) in HK-2 cells significantly ameliorated HG-induced inflammation, mitochondrial stress, and fatty acid synthesis. Molecular docking revealed that ACSS2 interacted with Sirtuin 1 (SIRT1). In HG-treated HK-2 cells, we demonstrated that ACSS2 suppressed SIRT1 expression and activated fatty acid synthesis by modulating SIRT1-carbohydrate responsive element binding protein (ChREBP) activity, leading to mitochondrial oxidative stress and inflammation. We conclude that ACSS2 promotes mitochondrial oxidative stress and renal tubular inflammation in DN by regulating the SIRT1-ChREBP pathway. This highlights the potential therapeutic value of pharmacological inhibition of ACSS2 for alleviating renal inflammation and dysregulation of fatty acid metabolic homeostasis in DN.

Keywords: diabetic nephropathy; renal tubular cell; Acetyl-CoA synthetase 2; SIRT1; ChREBP; fatty acid metabolism

Acta Pharmacologica Sinica (2024) 45:366–377; <https://doi.org/10.1038/s41401-023-01160-0>

INTRODUCTION

Diabetic nephropathy (DN) is a progressive microvascular complication associated with diabetes, wherein renal tubular injury plays a dual role as both a victim and contributor to DN progression [1, 2]. Recent evidence suggests that injury to proximal renal tubular epithelial cells (RTECs) occurs in the early stages of DN and persists throughout the disease process [3]. To better understand the pathogenic mechanisms underlying tubular injury and prevent renal damage in DN, novel studies and targeted treatments are needed. Chronic low-grade inflammation in the kidneys has been implicated in the pathogenesis of DN, with increased inflammatory cell infiltration and accumulation of inflammatory cytokines causing damage and ultimately promoting renal dysfunction [4, 5]. However, the origin of this inflammatory process remains unclear despite substantial evidence supporting its causative role in DN progression.

Interleukin-1 β (IL-1 β) has been identified as an initiator of the renal inflammatory response associated with DN [6, 7]. Interestingly, RTECs rather than immune cells are the primary source of

IL-1 β . In the diabetic kidneys, IL-1 β expression is significantly upregulated in RTECs, prompting further investigation into the potential mechanism underlying IL-1 β production in these cells. Although abnormalities in glucose and lipid metabolism, mitochondrial dysfunction, and oxidative stress form a vicious cycle that ultimately leads to renal inflammation and tubular dysfunction in DN [8, 9], the regulation of pro-inflammatory responses in RTECs by these metabolic changes remains poorly understood.

Acetyl-CoA synthetase 2 (ACSS2) is predominantly recognized as a vital catalytic enzyme responsible for the alternative pathway for acetyl-CoA synthesis [10]. Most studies on the pathogenic contributions of ACSS2 have focused on its pro-resolving effects, including those on autophagy and lysosome biogenesis [11, 12]. ACSS2 has also been shown to modulate lipid metabolism [13]. ACSS2-deficient mice with high-fat diet exhibiting reduced body weight and attenuated hepatic steatosis [11]. However, the pathogenic mechanisms of ACSS2 in RTECs of diabetic mice remain poorly characterized.

¹Department of Nephrology, Nanjing Drum Tower Hospital, the Affiliated Hospital of Medical School, Nanjing University, Nanjing 210008, China; ²Institute of Nephrology, Zhongda Hospital, School of Medicine, Southeast University, Nanjing 210009, China and ³Department of Nephrology, the Second Affiliated Hospital, School of Medicine, Zhejiang University, Hangzhou 310003, China

Correspondence: Chun-ming Jiang (guloujiang@sina.com) or Kun-ling Ma (klma@zju.edu.cn)

These authors contributed equally: Jian Lu, Xue-qi Li

Received: 15 May 2023 Accepted: 28 August 2023

Published online: 28 September 2023

Emerging evidence suggests that abnormal fatty acid metabolism exacerbates diabetic renal tubular dysfunction [14]. The present study was designed to explore the role of ACS2 in renal inflammation in DN. Mechanistically, ACS2 contributed to mitochondrial oxidative stress and inflammation by promoting ChREBP-mediated lipogenesis through interactions with Sirtuin 1 (SIRT1). We propose that ACS2-mediated regulation of fatty acid metabolism plays a distinct role in mitochondrial injury of RTECs and chronic renal inflammation in DN.

MATERIALS AND METHODS

Reagents

The following chemical reagents were utilized in this study: ACS2 inhibitor (Cat no: S8588, Selleck, Houston, Texas, USA); Streptozotocin (STZ, Cat no: S0130, Sigma, St. Louis, MO, USA); EX527 (Cat no: HY-15452, MedChemExpress, New Jersey, USA); Lotus Tetragonolobus Lectin (LTL, Cat no: FL-1321-2, ThermoFisher Scientific, Waltham, MA, USA); JC-1 (Cat no: C2006, Beyotime, Shanghai, China); dihydroethidium (DHE, Cat no: S0063, Beyotime, Shanghai, China); Reactive oxygen species (ROS) assay kit (Cat no: S00335, Beyotime, Shanghai, China); MitoSOX Red Mitochondrial Superoxide Indicator (Cat no: RM02822, Abclonal, Wuhan, Hubei, China); and 4, 4-difluoro-1, 3, 5, 7, 8-pentamethyl-4-bora-3a, 4a-diaza-s-indacene (BODIPY, Cat no: D3822, ThermoFisher Scientific, Waltham, MA, USA).

The following primary antibodies were employed in this study: anti-ACS2 (Cat no: ab133664) from Abcam (Cambridge, MA, UK); anti-kidney injury molecule1 (KIM-1, Cat no: sc-518008) from Santa Cruz (Dallas, Texas, USA); anti-IL-1 β (Cat no: 12242) and anti-SIRT1 (Cat no: 8469) from Cell Signaling Technology (Danvers, Massachusetts, USA); anti-adipophilin (ADRP, Cat no: 15294-1-AP); anti-fatty acid synthetase (FASN, Cat no: 10624-2-AP); ChREBP (Cat no: 13256-1-AP); carnitine palmitoyltransferase 1A (CPT1A, Cat no: 15184-1-AP) from Proteintech (Wuhan, Hubei, China); and anti-IL-6 (Cat no: DF6087) and anti-MCP-1 (Cat no: DF7577) from Affinity Biosciences (Changzhou, Jiangsu, China).

Human kidney tissue samples

The renal tissue samples from biopsy-proven DN patients from Nanjing Drum Tower Hospital were enrolled in this study. Control para-cancerous renal tissue samples were collected from individuals undergoing tumor nephrectomies, who displayed no clinical manifestations of diabetes or kidney disease. The study design adhered to the Declaration of Helsinki and received approval from the Ethics Committee of Nanjing Drum Tower Hospital, Affiliated Hospital of Medical School, Nanjing University.

Construction of the ACS2 gene knockout mouse model

Male C57BL/6J ACS2 knockout (ACS2 KO) mice were generated by GemPharmatech Biosciences Inc (Nanjing, Jiangsu, China). Real-time PCR determined genotyping for all mice. Male homozygous ACS2 KO transgenic mice and their wild-type littermate controls, aged 6–8 weeks, were included in subsequent modeling and observation. The animal experimental protocols were approved by the Review Committee of Nanjing University School of Medicine and adhered to institutional guidelines.

Diabetic mouse model

An experimental diabetic mice model was induced in 8-week-old wild-type and ACS2 KO mice via intraperitoneal injection of STZ. STZ (50 mg/kg body weight) was dissolved in sodium citrate buffer and administered intraperitoneally for five consecutive days. Control mice received vehicle citrate buffer at an equivalent dose. Mice with fasting glucose levels exceeding 16.7 mmol/L, two weeks post-STZ intervention, were considered diabetic and included in the study. The mice were then divided into four groups: control (Ctrl) ($n = 6$), ACS2 knockout (ACS2 KO) ($n = 5$), diabetes (DM) ($n = 6$), and ACS2 knockout diabetes (ACS2

KO + DM) ($n = 6$). The mice were humanely euthanized 12 weeks after STZ-induced successful modeling.

Immunofluorescent staining

Paraffin-embedded kidney sections were washed, and bovine serum albumin was applied to block nonspecific staining. Next, primary antibodies at appropriate concentrations were incubated at 4 °C overnight, followed by secondary antibodies conjugated with Alexa Fluor 594/488, which were applied at room temperature for one hour. After washing, sections were stained with DAPI and fluorescence intensity was detected.

Cell experiments

HK-2 cells were stimulated with D-glucose at a final concentration of 30 mmol/L for 24 h. Concurrently, cells were exposed to either the ACS2 inhibitor (10 μ mol/L) or EX527 (10 μ mol/L).

Small-interfering RNA transfection

HK-2 cells were transfected with ACS2 siRNA and scrambled siRNA, employing Lipofectamine 2000 transfection reagent. Scrambled siRNA was used as a negative control in the control group. The human ACS2 siRNA sequence (5'-CCTTCCACAATACGGAAATT-3') was chemically synthesized by GenePharma (Shanghai, China).

Real-time PCR

RNA was extracted from kidney tissues and HK-2 cells using TRIzol reagent. Equal amounts of RNA were employed for reverse-transcription PCR to generate cDNA, which was then amplified using a 7300 real-time PCR detection system (Applied Biosystems, USA). mRNA expression levels were analyzed using the $\Delta\Delta$ Ct method, with gene expression normalized to β -actin as an internal RNA control.

Western blot

Whole-cell extracts from kidney tissues and HK-2 cells were obtained by lysing cells in RIPA buffer containing phosphatase inhibitors, protease inhibitors, and phenylmethylsulfonyl fluoride (PMSF). Cell lysates were separated by sodium dodecyl sulfate-polyacrylamide gel electrophoresis (SDS-PAGE), transferred to polyvinylidene fluoride membranes, and subsequently probed with primary and secondary antibodies as previously described.

Reactive oxygen species (ROS) assay

The 2',7'-dichlorofluorescein diacetate (DCFH-DA) probe was diluted in serum-free cell culture medium. After medium removal, cells were incubated with DCFH-DA at 37 °C for one hour. The culture medium was then aspirated and replaced with serum-free medium, followed by fluorescence detection under FITC fluorescence detection conditions. DHE probes were employed to determine superoxide anion levels.

BODIPY staining

Cellular lipids were stained with BODIPY for 30 min, and then processed for immunofluorescence intensity detection according to a previously described method [15].

JC-1 staining

The JC-1 fluorescent probe was utilized to assess the mitochondrial membrane potential of HK-2 cells, as previously detailed [16]. HK-2 cells were seeded into 6-well plates at an appropriate density. Following supernatant removal, cells were incubated with JC-1 staining solution at 37 °C for 30 min. Subsequently, HK-2 cells were washed with JC-1 staining buffer and observed using a fluorescence microscope.

Mitochondrial ultrastructure detection

Kidney tissues were collected from mice and prepared for electron microscopy. The morphology of mitochondria in RTECs was examined as previously reported [17].

Statistical analysis

All data were presented as mean ± SD. Student's *t*-test or one-way ANOVA with Bonferroni correction was applied as appropriate. A *P*-value < 0.05 was deemed statistically significant. Data analysis was performed using GraphPad Prism version 7.0 (GraphPad Software Inc., San Diego, CA, USA).

RESULTS

Increased ACS2 expression in RTECs of diabetic mice and human individuals with DN

Transcriptomic data analysis from Humphreys Lab Single Cell Portal (<http://humphreyslab.com/SingleCell/>) [18] revealed that ACS2 was predominantly expressed in glomerular podocytes and RTECs (Fig. 1a). To explore the potential involvement of ACS2 in the pathogenesis of diabetic renal tubular injury, we examined its expression levels in diabetic kidneys. Co-localization of ACS2 with renal tubular injury biomarker KIM-1 was confirmed by immunofluorescence staining in the renal cortex isolated from human individuals with biopsy-proven DN (Fig. 1b). Accumulation of

inflammatory mediators, such as cytokine IL-1β, is known to promote renal dysfunction in DN. Compared to the control group, IL-1β expression in RTECs was significantly increased in the kidney of patients with DN (Fig. 1c). Consistent with human data, IL-1β expression in renal tubular tissues was more abundant in areas with elevated ACS2 expression in RTECs during DN (Fig. 1d). Western blot analysis further verified that ACS2 was significantly upregulated in the renal tissue of diabetic mice (Fig. 1e). Collectively, these findings suggest that ACS2 upregulation may contribute to IL-1β production and inflammation in RTECs during DN.

ACS2 contributes to mitochondrial oxidative stress and the inflammatory response in RTECs under high-glucose (HG) conditions in vitro

To further elucidate the pathogenic role of ACS2 in RTECs, HK-2 cells were subjected to either low (5.5 mmol/L) or HG (30 mmol/L) conditions for 24 h. HK-2 cells exposed to HG exhibited increased ACS2 expression, as demonstrated by immunofluorescent staining and Western blot analysis (Fig. 2a). Inhibition of ACS2 led to

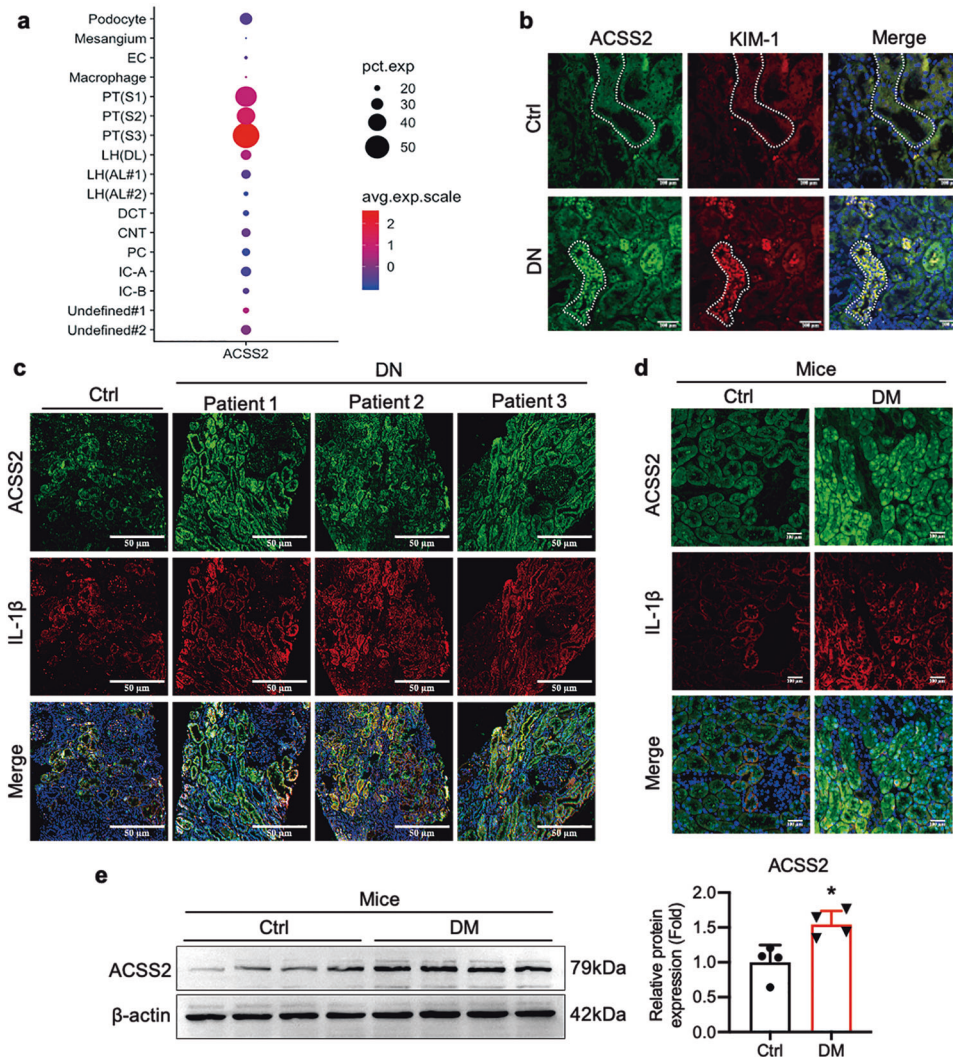


Fig. 1 ACS2 upregulation in renal tubular epithelial cells (RTECs) of in vivo murine STZ-induced diabetic models and patients with biopsy-proven DN. **a** Online transcriptome data revealed ACS2 predominantly expressed in renal podocytes and RTECs (EC endothelial cells, PT proximal tubule). **b** Immunofluorescence staining of kidney injury markers KIM-1 (red) and ACS2 (green), and DAPI (blue) in kidney sections from patients with biopsy-proven DN and the control. Scale bars, 100 μm. **c** Immunofluorescence staining of IL-1β (red) and ACS2 (green), and DAPI (blue) in kidney sections from patients with biopsy-proven DN and control individuals. Scale bars, 50 μm. **d** Immunofluorescence staining of IL-1β (red) and ACS2 (green), and DAPI (blue) in kidney sections from diabetic mice and control group. Scale bars, 100 μm. **e** ACS2 protein expression in the kidneys from diabetic mice and control mice. Mean ± SD. *n* = 4, **P* < 0.05 vs. Ctrl.

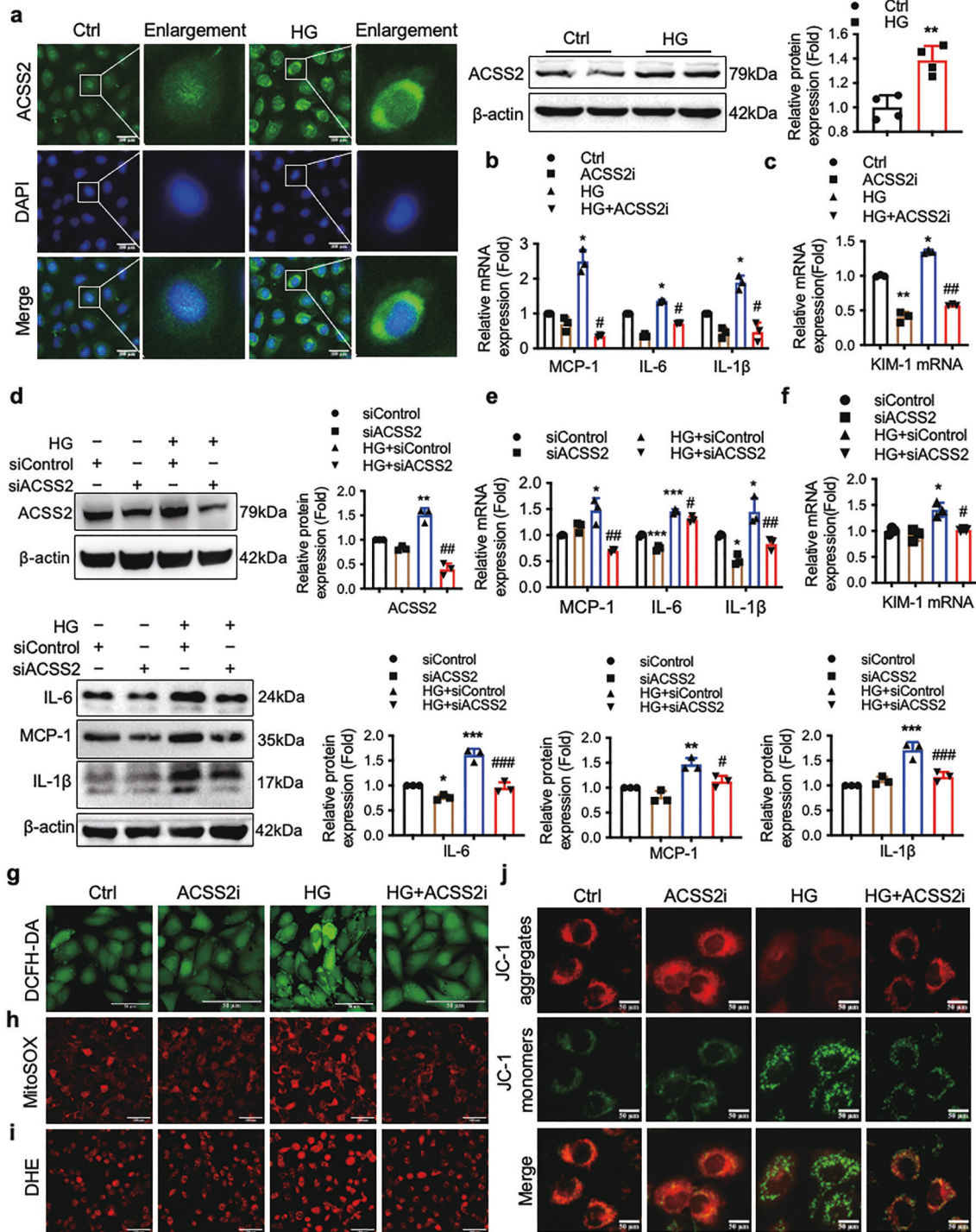


Fig. 2 ACS2's role in the inflammatory response and mitochondrial oxidative stress in HK-2 cells under HG challenges. For (a–c) and (g–j), HK-2 cells were treated for 24 h with HG (30 mmol/L) with or without ACS2 inhibitor (ACSS2i, 10 μmol/L). Mean ± SD. *n* = 3, **P* < 0.05, ***P* < 0.01 vs. Ctrl, #*P* < 0.05, ##*P* < 0.01 vs. HG. **a** ACS2 protein expression in HK-2 cells determined by immunofluorescence staining with ACS2 (green) and DAPI (blue). Scale bars, 100 μm. **b, c** mRNA expression of pro-inflammatory factors MCP-1, IL-1β, IL-6, and kidney injury marker KIM-1 in HK-2 cells. For (d–f), HK-2 cells were transfected with ACS2 siRNA (siRNA) or negative control siRNA (siControl) after treatment with HG (30 mmol/L) for 24 h. Mean ± SD. *n* = 3, **P* < 0.05, ***P* < 0.01, ****P* < 0.001 vs. siControl; #*P* < 0.05, ##*P* < 0.01 vs. HG+siControl. **d** Western blot analysis of ACS2 protein expression in HK-2 cells confirming ACS2 knockdown by specific siRNA. **e** Relative mRNA and protein expression of MCP-1, IL-1β, and IL-6 in ACS2-deficient HK-2 cells compared to control. **f** Relative mRNA expression of KIM-1 in HK-2 cells. **g–i** DCFH-DA (g), MitoSOX Red (h), and DHE staining (i) of HK-2 cells. Scale bars, 50 or 100 μm. **j** Mitochondrial membrane potential staining (JC-1) was detected in HK-2 cells. Scale bars, 50 μm.

decreased mRNA expression of pro-inflammatory factors (MCP-1, IL-6, and IL-1 β) and renal injury marker KIM-1 in HG-induced HK-2 cells (Fig. 2b, c). We also employed ACSS2 siRNA to knock down ACSS2 expression, confirming specific knockdown of ACSS2 at the protein level (Fig. 2d). Consistently, pro-inflammatory factors (MCP-1, IL-6, and IL-1 β) (Fig. 2e) and renal injury marker KIM-1 (Fig. 2f) expression levels were reduced by ACSS2 siRNA.

We further assessed the impact of ACSS2 on mitochondrial oxidative stress in HK-2 cells. DCFH-DA staining demonstrated increased ROS levels in HG-treated HK-2 cells compared to vehicle control cells, which were reduced upon ACSS2 inhibition (Fig. 2g). Mitochondrial ROS levels in HK-2 cells were determined using the fluorogenic dye MitoSOX Red, revealing a significant increase in red fluorescence intensity following HG exposure (Fig. 2h). Dihydroethidium (DHE) staining, which exhibits red nuclear fluorescence when oxidized by ROS, displayed increased fluorescence intensity in HG-treated HK-2 cells, while ACSS2 knockdown reduced this intensity (Fig. 2i). JC-1 staining was employed to detect mitochondrial membrane potential, with a transition from red to green fluorescence indicating decreased membrane potential. This transition was observed in HG-treated HK-2 cells and was inhibited upon ACSS2 suppression (Fig. 2j). In summary, these results demonstrate that ACSS2 promotes inflammatory response and mitochondrial oxidative stress in RTECs under HG conditions.

ACSS2 deletion protects against diabetes-induced renal tubular injury, mitochondrial oxidative stress, and inflammation

To elucidate the role of ACSS2 in diabetes-induced renal tubular injury, ACSS2 knockout (ACSS2 KO) mice were generated by deleting the ACSS2 gene. Both ACSS2 KO mice and their wild-type littermates were used to establish a diabetic mouse model, which was induced by administering intraperitoneal injections of STZ (50 mg/kg) for five consecutive days. Mice were sacrificed 12 weeks after successful model establishment (Fig. 3a). Notably, a significant decrease in ACSS2 expression was observed in the kidneys of ACSS2 KO mice, especially in the renal tubules (Fig. 3b, c). At baseline, no kidney morphological abnormalities were observed in ACSS2 KO mice as determined by Periodic Acid-Schiff (PAS) staining. In comparison to diabetic wild-type mice, diabetic mice with ACSS2 deletion exhibited reduced renal tubular injury (Fig. 3d). Furthermore, protein expression of apical kidney injury molecule-1 (KIM-1), as assessed by immunofluorescent staining, was increased in RTECs of diabetic mice but significantly down-regulated in diabetic kidneys with ACSS2 deletion (Fig. 3e). Consistently, mRNA expression of KIM-1 and neutrophil gelatinase-associated lipocalin (NGAL) was upregulated in diabetic mouse kidneys 12 weeks post-induction but decreased in ACSS2-deleted diabetic kidneys (Fig. 3f).

Previous studies have demonstrated that mitochondrial dysfunction-mediated ROS production contributes to inflammation. Therefore, we investigated the protective effects of ACSS2 deficiency on mitochondrial deficits in diabetic mice. As shown in Fig. 3g, no morphological differences in mitochondria were observed in the renal tubule epithelium of ACSS2 KO mice compared to wild-type mice. However, following diabetes induction, mitochondrial fragmentation, swelling, loss of cristae, and vacuoles in the mitochondrial matrix were observed in RTECs of wild-type diabetic mice. These abnormalities were dramatically ameliorated in ACSS2-deficient diabetic kidneys, indicating that ACSS2 deficiency mitigated mitochondrial dysfunction and kidney tubular injuries in diabetic mice. Our preliminary *in vitro* study suggested that ACSS2 promoted the conversion of RTECs to a pro-inflammatory phenotype. Consequently, we sought to determine whether the absence of ACSS2 in STZ-induced diabetic mice was associated with ameliorated renal tubular cell inflammation. Indeed, diabetic mice exhibited increased MCP-1, IL-6, and IL-1 β MCP-1 mRNA or protein expression in the kidney compared to

control mice, which were significantly decreased in diabetic mice with ACSS2 KO (Fig. 3h–j). Collectively, these findings demonstrate the detrimental role of ACSS2 in mitochondrial injury and inflammation of RTECs in diabetic mice.

ACSS2 deficiency mitigates fatty acid accumulation in RTECs of diabetic mice

Previous studies have established that ACSS2 modulates fatty acid metabolism. Thus, we investigated the impact of ACSS2 deletion on fatty acid accumulation in the RTECs of diabetic mice. Oil red O staining revealed that ACSS2 deletion diminished lipid accumulation in the kidneys, compared to the diabetic model group (Fig. 4a). Adipose differentiation-related protein adipophilin (ADRP) is localized on lipid droplets, with its expression abundance reflecting the degree of lipid droplet accumulation [19]. ADRP immunofluorescence staining results demonstrated substantial lipid deposition in the RTECs of diabetic mice, which was reduced in diabetic mice lacking the ACSS2 gene (Fig. 4b). In line with *in vivo* findings, ACSS2 inhibitor treatment curtailed lipid droplet accumulation in HG-treated HK-2 cells, as evidenced by BODIPY staining (Fig. 4c). Collectively, these findings indicate that ACSS2 depletion alleviates excessive intrarenal fatty acid accumulation in diabetic mouse kidneys and HG-induced HK-2 cells.

ACSS2 inhibition mitigates fatty acid synthesis-related gene expression in HG-treated RTECs

Cellular metabolic reprogramming plays a crucial role in supporting the inflammatory phenotype. We speculated that ACSS2 fosters inflammation by altering the fatty acid metabolic pattern of RTECs. Considering ACSS2's role in driving adipogenesis and renal tubular cells' reliance on fatty acid oxidation for energy, we examined cellular fatty acid metabolic homeostasis, regulated by fatty acid uptake, *de novo* synthesis, and oxidation processes (Fig. 5a) [20]. To elucidate the mechanisms underlying HG-induced lipid accumulation, we assessed the expression of key lipogenic genes, fatty acid synthetase (FASN), acetyl-CoA carboxylase (ACC), and stearoyl-CoA desaturase1 (SCD1) in HK-2 cells. Interestingly, HG treatment upregulated FASN, ACC, and SCD1 expression, which was significantly suppressed by ACSS2 inhibition. Moreover, ACSS2 inhibition restored carnitine palmitoyltransferase 1A (CPT1A) expression but did not significantly affect fatty acid uptake-related gene expression of FATP2 and CD36 (Fig. 5b, c).

Carbohydrate response-element-binding protein (ChREBP) is an essential transcription factor regulating fatty acid metabolism gene expression. Our *in vitro* and *in vivo* findings also suggest that ACSS2 positively modulates ChREBP expression (Fig. 5c, d). Immunofluorescence staining and Western blot analysis of mouse-based experiments further corroborated these observations. Consequently, ACSS2 gene knockout significantly decreased ChREBP and FASN expression while increasing CPT1A expression in the kidneys (Fig. 5d, e). Overall, these data demonstrate that ACSS2 stimulates lipogenesis and suppresses fatty acid oxidation during the pro-inflammatory process in diabetes-induced RTECs.

ACSS2 interacts with SIRT1 and suppresses SIRT1 expression

In the context of chronic hyperglycemia-induced energy overload, the precise role of ACSS2-mediated metabolic reprogramming in modulating ChREBP activity remained elusive. Given that the deacetylase SIRT1 serves as a key upstream metabolic regulator activated in response to energy stress [21], we focused on its potential involvement. Prior research has demonstrated an interaction between SIRT1 and ChREBP [22], prompting us to investigate whether SIRT1 participates in ACSS2-induced ChREBP expression. We analyzed molecular docking data for ACSS2 on SIRT1 using the AutoDock software (<https://www.rcsb.org>) (Fig. 6a). SIRT1 protein expression levels were found to be reduced in diabetic kidneys and in HK-2 cells treated with HG (Fig. 6b). Deletion and the inhibition of ACSS2 led to an increase in SIRT1

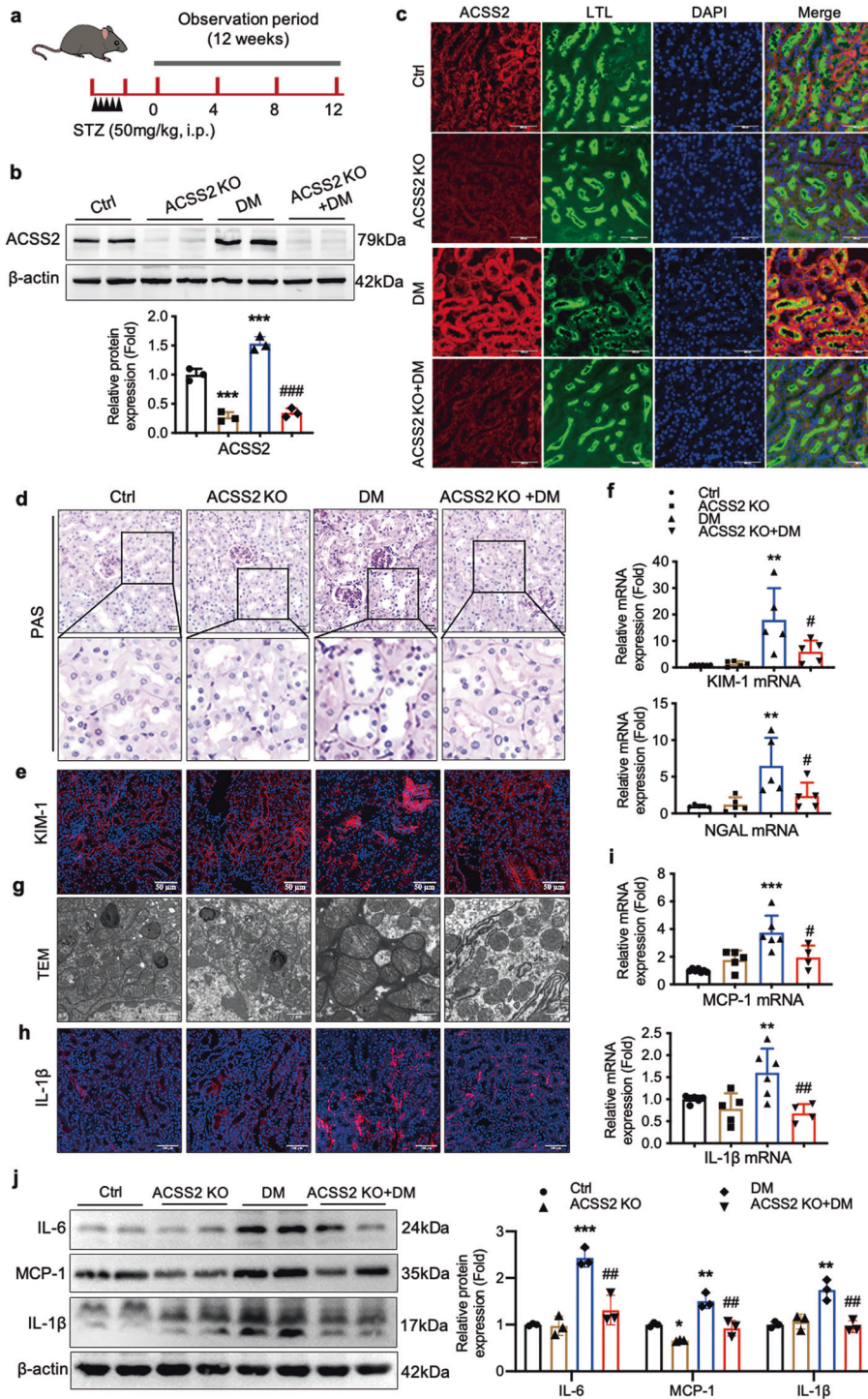


Fig. 3 ACSS2 deletion protects against diabetes-induced renal tubular injury, mitochondrial oxidative stress, and inflammation. The ACSS2 knockout (KO) and wild-type mice were selected for modeling. The diabetes mouse model was constructed by intraperitoneal injection of STZ (50 mg/kg) for five consecutive days, and the mice were sacrificed in the 12th week after successful modeling. $n = 5-6$, $^{***}P < 0.01$, $^{****}P < 0.001$ vs. Ctrl, $^{\#}P < 0.05$, $^{\#\#}P < 0.01$ vs. DM. **a** A schematic representation of the mouse model. **b** Representative Western blot images and densitometric analysis of ACSS2 protein expression in the renal cortex of mice. Mean \pm SD, $n = 3$. **c** Immunofluorescent staining of ACSS2 and Lotus Tetragnolobus Lectin (LTL) in mouse kidneys. Scale bars, 200 μ m. **d** Representative sections of PAS staining of kidney tissues. Scale bars, 20 μ m. **e** Representative images for immunofluorescence staining showing KIM-1 expression. Scale bars, 50 μ m. **f** mRNA levels of KIM-1 and NGAL in mouse renal cortices. **g** Representative transmission electron microscopy (TEM) images of renal tubular mitochondria from different groups of mice. Scale bars, 1 μ m. **h** Representative immunofluorescent staining of IL-1 β in mouse kidneys. Scale bars, 200 μ m. **i, j** The mRNA and protein levels of MCP-1, IL-1 β and IL-6 in mouse renal cortices. Mean \pm SD, $n = 3$.

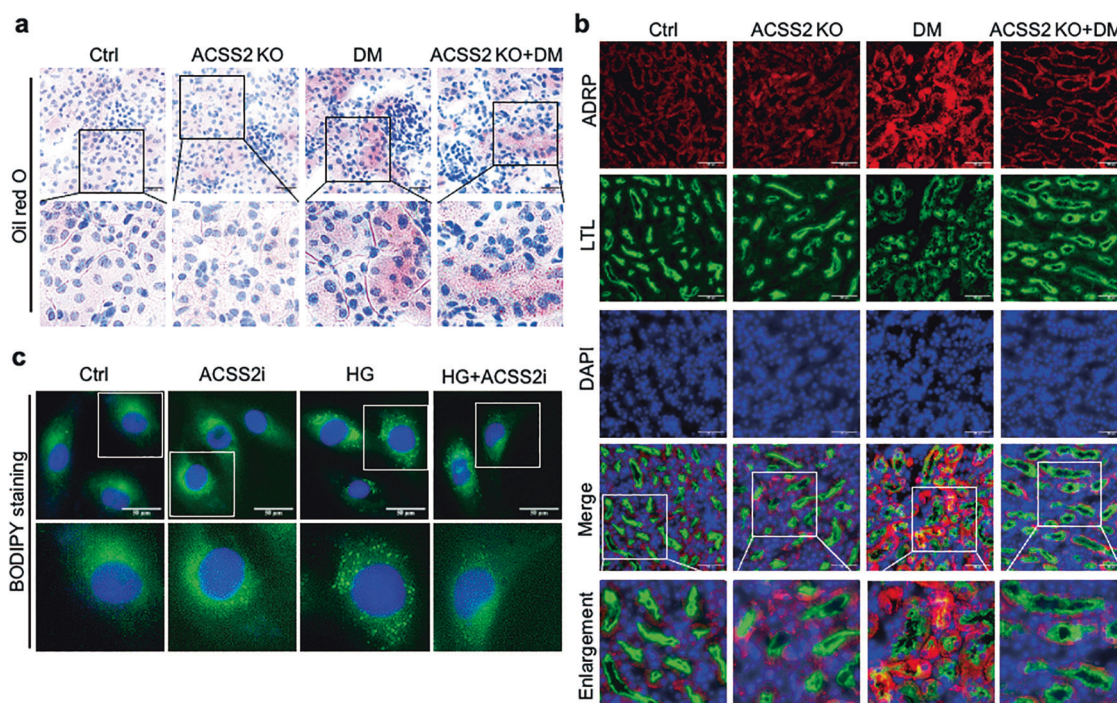


Fig. 4 ACSS2 deficiency reduced fatty acid accumulation in RTECs of diabetic mice. **a** Representative Oil Red O staining images of mouse kidneys. Scale bars, 200 μ m. **b** Immunofluorescent staining of adipose differentiation-related protein adipophilin (ADRP) (red) and Lotus Tetragonolobus Lectin (LTL, green) in mouse kidneys. Scale bars, 200 μ m. **c** Representative BODIPY immunofluorescence staining images in HK-2 cells. Scale bars, 50 μ m.

expression in HG-induced HK-2 cells (Fig. 6c, d) and RTECs of diabetic mice (Fig. 6e, f). Thereby, ACSS2 interacts with SIRT1 to suppress SIRT1 activity.

ACSS2 promotes inflammation and mitochondrial oxidative stress by suppressing SIRT1 activity

As we have demonstrated, SIRT1 is a downstream target of ACSS2. We wanted to investigate whether SIRT1 mediates ACSS2-induced mitochondrial oxidative stress and inflammation in RTECs under HG treatment conditions. To this end, we inhibited ACSS2 activity in HK-2 cells and then treated them with the SIRT1 inhibitor EX527. We found that the inhibition of SIRT1 partially rescued the expression of both ChREBP and FASN. Moreover, EX527 partially reversed the restoration of CPT1A expression that was mediated by ACSS2 inhibition in HG-treated HK-2 cells (Fig. 7a). The beneficial effect of inhibiting ACSS2 activity on inflammation and mitochondrial oxidative stress in HG-treated HK-2 cells was partially reversed by EX527 (Fig. 7b, c). Collectively, our findings suggest that ACSS2 interacts with SIRT1 to facilitate ChREBP-dependent lipogenesis and CPT1A suppression, thereby promoting inflammation and mitochondrial oxidative stress in RTECs under diabetes conditions.

DISCUSSION

Renal inflammation plays a pivotal role in the development of DN in both human and animal models; however, the underlying mechanisms initiating and propagating the inflammatory response remain largely elusive. In this study, we propose a novel molecular mechanism involving ACSS2 in the dysfunction of fatty acid metabolism, mitochondrial oxidative stress, and renal tubular inflammation during DN. Our data robustly demonstrate that ACSS2, an enzyme mainly expressed in RTECs, significantly co-localizes with pro-inflammatory cytokine IL-1 β , thereby establishing a molecular link between fatty acid metabolic reprogramming and inflammation in the kidney during DN.

The primary biological function of ACSS2 is to convert acetate and CoA into acetyl-CoA [10]. Few studies have established a pathogenetic connection between ACSS2 and chronic inflammatory diseases such as DN. Recent findings showed that diet-induced obese mice with ACSS2 deletion exhibited a lean phenotype and substantial improvement in hepatic steatosis due to reduced lipid transportation and enhanced lipid utilization [11]. Notably, ACSS2 co-localized with renal injury marker KIM-1, and ACSS2 upregulation was corroborated by immunofluorescence staining in renal cortex samples from individuals with biopsy-proven DN. These findings prompted further investigation into the potential relationship between ACSS2 upregulation and RTECs damage in DN.

Traditionally, hyperglycemia has been considered the main driver of chronic inflammation in type 2 diabetes; however, recent evidence indicates that the interplay between fatty acid metabolism imbalance and mitochondrial dysfunction is the primary cause of chronic inflammation in type 2 diabetes [23, 24]. Metabolically driven IL-1 β production initiates chronic sterile inflammation and exacerbates diabetes-associated macrovascular and microvascular complications. Fatty acids have been shown to induce IL-1 α -mediated vascular inflammation by uncoupling mitochondrial respiration, thereby substantially eliciting IL-1 β production and diabetic vascular inflammation [25]. These findings highlight a crucial connection between cellular metabolic stress and innate inflammatory responses. Recent evidence also demonstrated that RTECs are the primary sources of IL-1 β in diabetic kidneys. IL-1 β can sustain the pro-inflammatory phenotype of macrophages and promote renal accumulation of pro-inflammatory cytokines, ultimately increasing salt sensitivity in diabetic mice [26]. In line with these observations, our findings provide evidence that ACSS2 contributes to IL-1 β expression in RTECs and diabetic renal inflammation. These results suggest that pharmacological inhibition of ACSS2 may represent a promising therapeutic strategy for DN and other chronic inflammatory diseases.

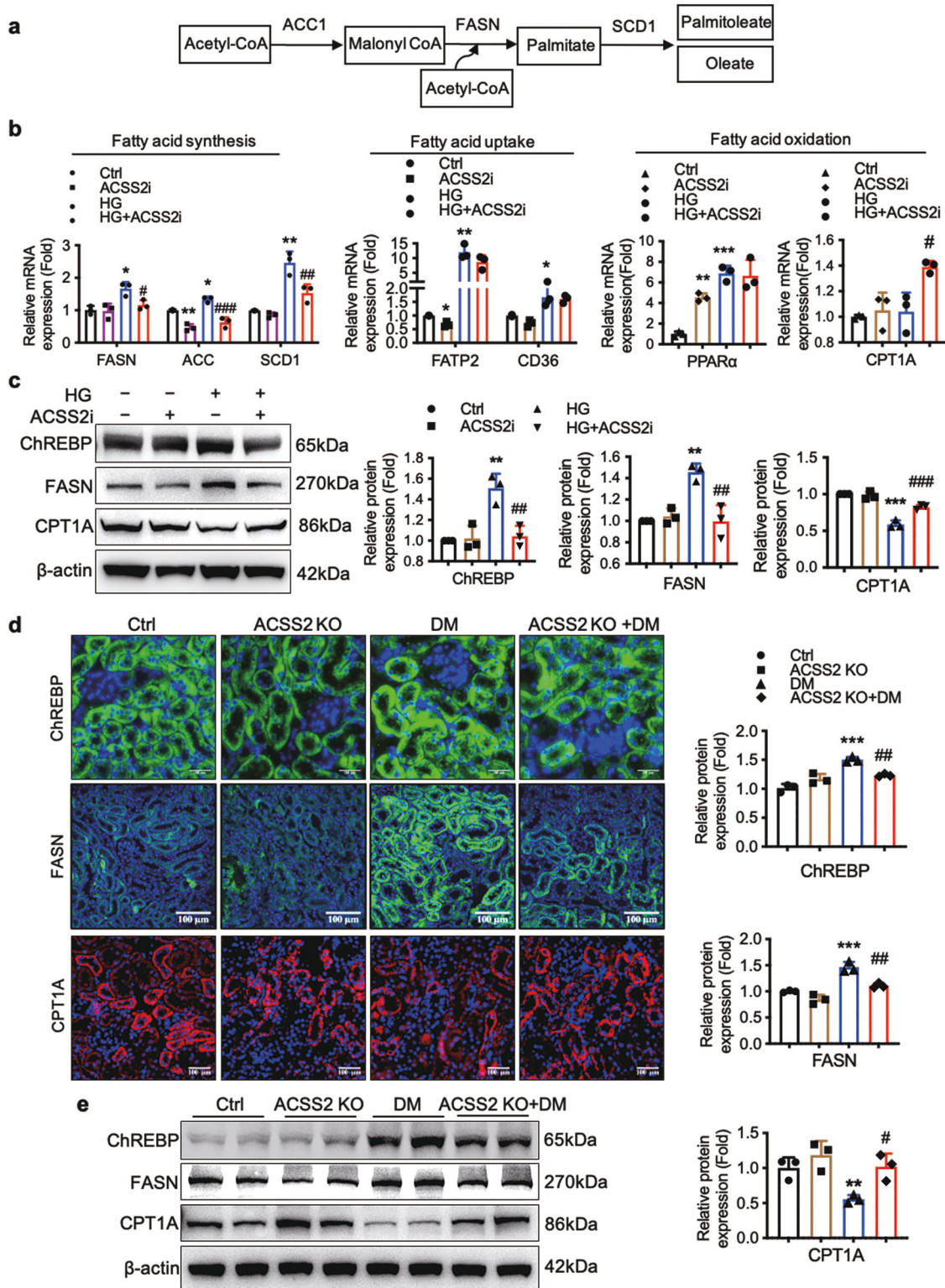


Fig. 5 ACSS2 inhibition reduced fatty acid synthesis-related gene expression in diabetic mice and HG-treated HK-2 cells. **a** A brief summary of the key steps in fatty acid synthesis and related metabolic enzymes. **b** and **c** HK-2 cells were treated with a specific ACSS2 inhibitor (10 μ mol/L) followed by stimulation with HG for 24 h. Mean \pm SD. $n = 3$, $^*P < 0.05$, $^{**}P < 0.01$, $^{***}P < 0.001$ vs. Ctrl, $^{\#}P < 0.05$, $^{\#\#}P < 0.01$, $^{\#\#\#}P < 0.001$ vs. HG. **b** Relative mRNA levels of key lipogenic genes (FASN, ACC, and SCD1), essential fatty acid uptake genes (FATP2 and CD36), and two key lipolysis enzymes (PPAR α and CPT1A). **c** Protein levels of ChREBP, FASN, and CPT1A. **d** and **e** Representative immunofluorescence staining images and Western blot detection of ChREBP, FASN, and CPT1A in kidney tissues. Scale bars, 100 μ m. Mean \pm SD. $n = 3$, $^{**}P < 0.01$, $^{***}P < 0.001$ vs. Ctrl; $^{\#}P < 0.05$, $^{\#\#}P < 0.01$ vs. DM.

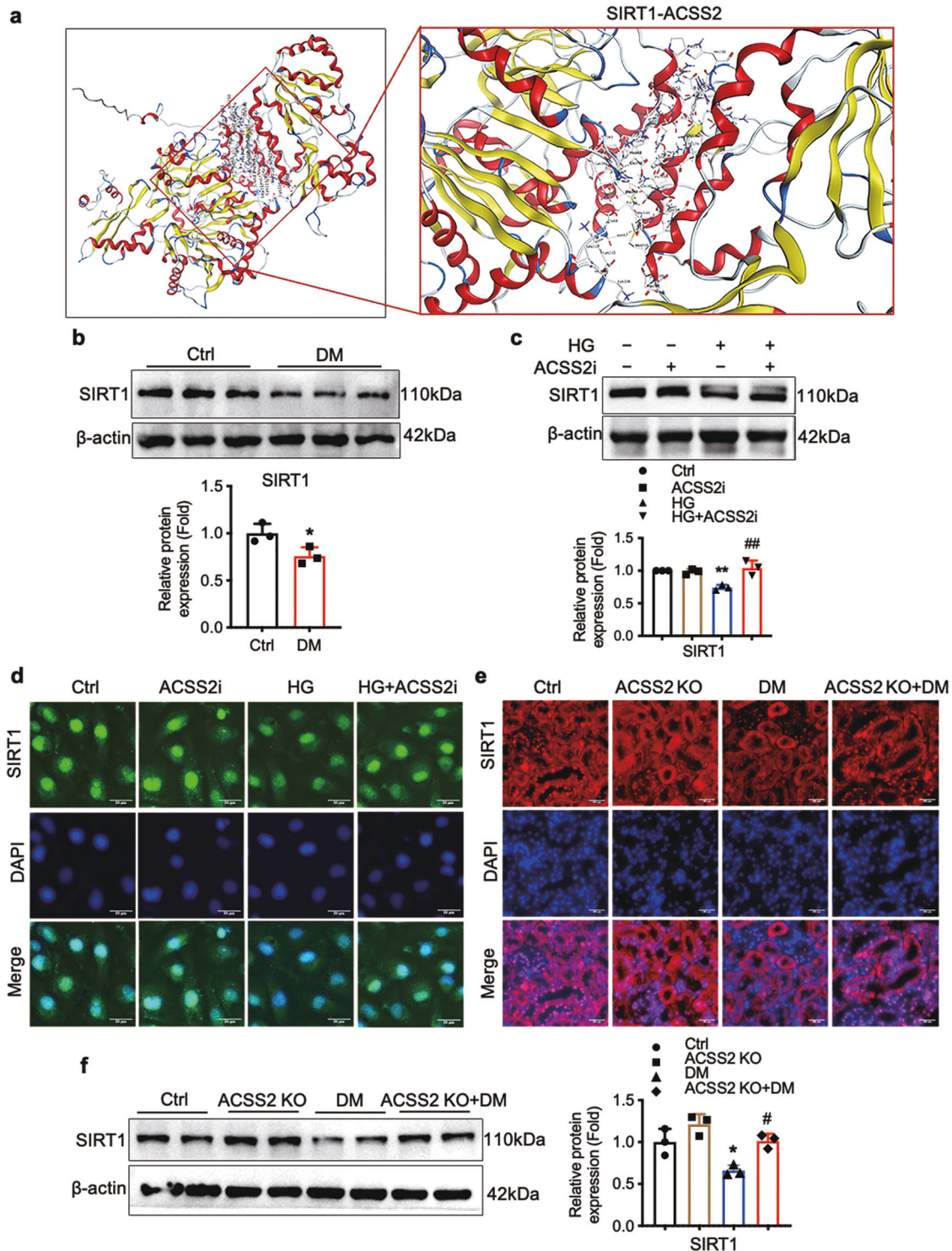


Fig. 6 ACS2 interacts with SIRT1 and suppresses SIRT1 expression. **a** Molecular docking analysis of ACS2 and SIRT1 using autodocking software. **b** SIRT1 protein expression in the kidneys of the diabetic and control mice. $n = 3$, $^*P < 0.05$ vs. Ctrl. **c** SIRT1 protein expression in HK-2 cells transfected with the ACS2 inhibitor (10 μ mol/L) followed by stimulation with HG for 24 h. Mean \pm SD. $n = 3$, $^{**}P < 0.01$ vs. Ctrl, $^{##}P < 0.01$ vs. HG. **d** Representative immunofluorescence staining images of SIRT1 in HK-2 cells. Scale bars, 50 μ m. **e** Representative immunofluorescence staining images of SIRT1 (red) and DAPI (blue) in kidney tissues. Scale bars, 100 μ m. **f** SIRT1 protein expression in the kidneys from different groups of mice. Mean \pm SD. $n = 3$, $^*P < 0.05$ vs. Ctrl; $^{\#}P < 0.05$ vs. DM.

Indeed, lipid derivatives known as fatty acids are critical for cellular energy metabolism and normal structure [27, 28]. However, excess free fatty acids, generated through the upregulation of fatty acid synthesis, might promote IL-1 β production by inducing the production of ROS and impairing mitophagy

[29, 30]. Increased lipid metabolism is a notable metabolic pathway in M1-like pro-inflammatory macrophages. The reprogramming of fatty acid metabolism guides immune functions, including NLRP3 inflammasome activation. Ceramide, a lipid derivative, activates IL-1 β production in macrophages by

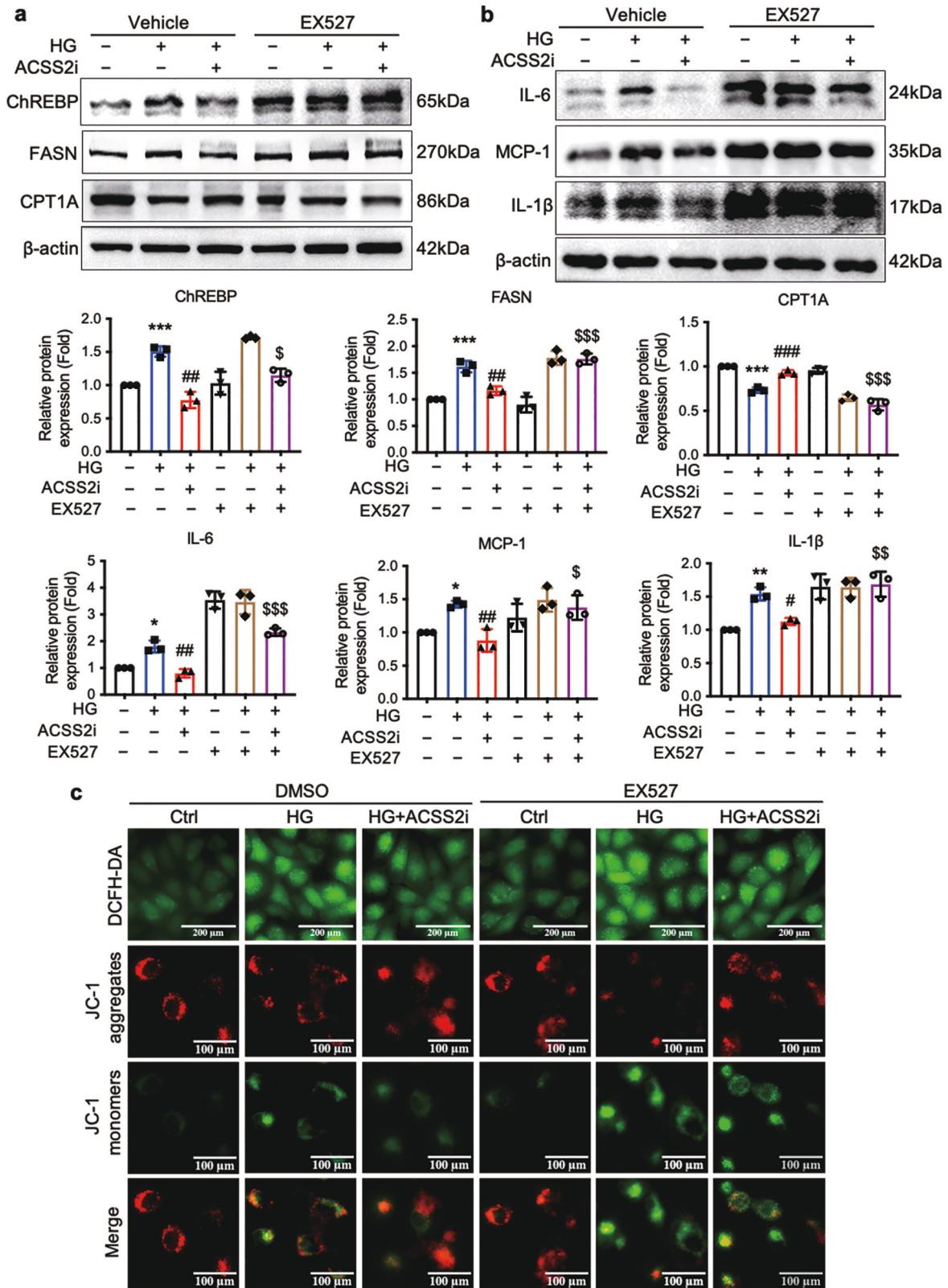


Fig. 7 ACSS2 promoting inflammation and mitochondrial oxidative stress of RTECs by suppressing SIRT1 activity. The SIRT1 inhibitor EX527 reverses the effect of ACSS2 inhibitor in HG-treated HK-2 cells. $n = 3$, $*P < 0.05$, $**P < 0.01$, $***P < 0.001$ vs. Ctrl; $\#P < 0.05$, $\#\#P < 0.01$, $\#\#\#P < 0.001$ vs. HG; $^{\$}P < 0.05$, $^{\$ \$}P < 0.01$, $^{\$ \$ \$}P < 0.001$ vs. HG+ACSS2i. **a** Relative protein expression of ChREBP, FASN, and CPT1A in HK-2 cells. **b** Relative protein expression of MCP-1, IL-1β, and IL-6 in HK-2 cells. **c** DCFH-DA and JC-1 staining was detected in HK-2 cells. Scale bars, 200 or 100 μm.

modulating oxidative stress during obesity-induced chronic inflammation [29]. Furthermore, fatty acid metabolism alters membrane lipid compositions, subsequently stimulating TLR4 signaling in immune cells [31]. Notably, fatty acid synthesis is a characteristic feature of the inflammatory response in both innate and adaptive immune systems. FASN is the only enzyme that converts acetyl-CoA and malonyl-CoA into palmitate, and excessive palmitate synthesis serves as a crucial driving factor of cellular metabolic dysfunction. The FASN inhibitor ASC40 prevented the release of pro-inflammatory cytokines, reduced metabolic parameters, and hepatic histological severity scores in a diet-induced NASH mouse model. These results suggest that the inhibition of FASN is an effective strategy to improve organ lipid deposition and mitigate pathological damages [32]. In this study, we established a robust association between ACS2, fatty acid synthesis, and inflammation. We discovered that hyperglycemia stimulation in RTECs induced fatty acid anabolism disorder mediated by ACS2 activation, thereby controlling the inflammatory response. This finding reinforces the link between fatty acid anabolism and metabolic inflammation in diabetic RTECs. We identified a previously unreported RTECs response to ACS2 that is mainly specific to the fatty acid-inflammation signaling pathways.

Previous research has suggested that ACS2 may be a critical enzyme for the interplay between glucose and lipid metabolism disorders [33]. Fructose intake has been shown to promote intestinal acetate synthesis, subsequently triggering liver lipid synthesis in a microbial fermentation-dependent manner. However, when antibiotics were used to interfere with the microbiome's fermentation to produce acetate, hepatic lipid synthesis was inhibited [34]. Our prior work also demonstrated a significant increase in plasma acetate levels in diabetic rats [35]. In the present study, upregulation of ACS2 expression promoted ChREBP-mediated fatty acid synthesis and renal inflammation in diabetic RTECs. Based on these findings, we hypothesize that an imbalance in the intestinal microbiota promotes acetate production in diabetic mice, serving as a substrate for ACS2 and driving ACS2-mediated renal fatty acid synthesis. The specific regulatory mechanism by which intestinal microbiota drives acetate synthesis and activates ACS2 in RTECs under diabetic conditions, however, requires further clarification.

In summary, our findings reveal that genetic deletion of ACS2 mitigates renal tubular injuries and inflammation in diabetic mice. Mechanistically, ACS2 promotes fatty acid metabolism disorder and mitochondrial oxidative stress. This study provides a novel perspective on the contribution of ACS2 to metabolic inflammation and disease progression in DN. Furthermore, our results suggest that pharmacological inhibition of ACS2 holds potential therapeutic promise for DN and other inflammatory diseases.

DATA AVAILABILITY

Data supporting the concepts presented in this manuscript can be obtained upon reasonable request from the corresponding author.

ACKNOWLEDGEMENTS

This research was supported by the Jiangsu Innovative and Entrepreneurial Talent Programme (JSSCBS20211515), the Nanjing Postdoctoral Science Foundation, the Medical Science and Technology Development Foundation's Key Project, Nanjing Department of Health (YKK21094), and the National Natural Science Foundation of China (82170736, 81970629). This research did not use artificial intelligence, language models, machine learning, or similar technologies to create content or assist with the writing or editing of manuscripts.

AUTHOR CONTRIBUTIONS

The study was designed by JL and KLM. The experiments were conducted and diabetic mouse models established by JL, XQL, PPC, JXZ, and LL. Data analysis was

performed by GHW and XQL. The manuscript was initially drafted by JL, while revisions were made by KLM and CMJ. All authors have approved the final version of the manuscript. Guarantor statement: KLM and CMJ have taken responsibility for the contents of the manuscript.

ADDITIONAL INFORMATION

Competing interests: The authors declare no competing interests.

REFERENCES

- Zeni L, Norden AGW, Cancarini G, Unwin RJ. A more tubulocentric view of diabetic kidney disease. *J Nephrol.* 2017;30:701–17.
- Ruiz-Ortega M, Rodrigues-Diez RR, Lavozy C, Rayego-Mateos S. Special Issue "Diabetic Nephropathy: Diagnosis, Prevention and Treatment". *J Clin Med.* 2020;9:813.
- Nowak N, Skupien J, Niewczas MA, Yamanouchi M, Major M, Croall S, et al. Increased plasma kidney injury molecule-1 suggests early progressive renal decline in non-proteinuric patients with type 1 diabetes. *Kidney Int.* 2016;89:459–67.
- Vallon V, Thomson SC. The tubular hypothesis of nephron filtration and diabetic kidney disease. *Nat Rev Nephrol.* 2020;16:317–36.
- Tang SC, Lai KN. The pathogenic role of the renal proximal tubular cell in diabetic nephropathy. *Nephrol Dial Transpl.* 2012;27:3049–56.
- Tang SCW, Yiu WH. Innate immunity in diabetic kidney disease. *Nat Rev Nephrol.* 2020;16:206–22.
- Veiras LC, Bernstein EA, Cao D, Okwan-Duodu D, Khan Z, Gibb DR, et al. Tubular IL-1 β induces salt sensitivity in diabetes by activating renal macrophages. *Circ Res.* 2022;131:59–73.
- Lumeng CN, Saltiel AR. Inflammatory links between obesity and metabolic disease. *J Clin Invest.* 2011;121:2111–7.
- Ding H, Li J, Li Y, Yang M, Nie S, Zhou M, et al. MicroRNA-10 negatively regulates inflammation in diabetic kidney via targeting activation of the NLRP3 inflammasome. *Mol Ther.* 2021;29:2308–20.
- Gao X, Lin SH, Ren F, Li JT, Chen JJ, Yao CB, et al. Acetate functions as an epigenetic metabolite to promote lipid synthesis under hypoxia. *Nat Commun.* 2016;7:11960.
- Huang Z, Zhang M, Plec AA, Estill SJ, Cai L, Repa JJ, et al. ACS2 promotes systemic fat storage and utilization through selective regulation of genes involved in lipid metabolism. *Proc Natl Acad Sci USA.* 2018;115:E9499–506.
- Li X, Qian X, Lu Z. Local histone acetylation by ACS2 promotes gene transcription for lysosomal biogenesis and autophagy. *Autophagy.* 2017;13:1790–1.
- Lakhter AJ, Hamilton J, Konger RL, Brustovetsky N, Broxmeyer HE, Naidu SR. Glucose-independent acetate metabolism promotes melanoma cell survival and tumor growth. *J Biol Chem.* 2016;291:21869–79.
- van der Rijt S, Leemans JC, Florquin S, Houtkooper RH, Tammaro A. Immuno-metabolic rewiring of tubular epithelial cells in kidney disease. *Nat Rev Nephrol.* 2022;18:588–603.
- Lu J, Chen PP, Zhang JX, Li XQ, Wang GH, Yuan BY, et al. GPR43 activation-mediated lipotoxicity contributes to podocyte injury in diabetic nephropathy by modulating the ERK/EGR1 pathway. *Int J Biol Sci.* 2022;18:96–111.
- Guo Y, Ni J, Chen S, Bai M, Lin J, Ding G, et al. MicroRNA-709 mediates acute tubular injury through effects on mitochondrial function. *J Am Soc Nephrol.* 2018;29:449–61.
- Wu L, Liu C, Chang DY, Zhan R, Zhao M, Man Lam S, et al. The attenuation of diabetic nephropathy by Annexin A1 via regulation of lipid metabolism through the AMPK/PPAR α /CPT1b pathway. *Diabetes.* 2021;70:2192–203.
- Wu H, Uchimura K, Donnelly EL, Kirita Y, Morris SA, Humphreys BD. Comparative analysis and refinement of human PSC-derived kidney organoid differentiation with single-cell transcriptomics. *Cell Stem Cell.* 2018;23:869–81.e868.
- Herman-Edelstein M, Scherzer P, Tobar A, Levi M, Gafter U. Altered renal lipid metabolism and renal lipid accumulation in human diabetic nephropathy. *J Lipid Res.* 2014;55:561–72.
- Opazo-Rios L, Mas S, Marin-Royo G, Mezzano S, Gomez-Guerrero C, Moreno JA, et al. Lipotoxicity and diabetic nephropathy: novel mechanistic insights and therapeutic opportunities. *Int J Mol Sci.* 2020;21:2632.
- Qi W, Hu C, Zhao D, Li X. SIRT1-SIRT7 in diabetic kidney disease: biological functions and molecular mechanisms. *Front Endocrinol (Lausanne).* 2022;13:801303.
- Zhang N, Hu Y, Ding C, Zeng W, Shan W, Fan H, et al. Salvianolic acid B protects against chronic alcoholic liver injury via SIRT1-mediated inhibition of CRP and ChREBP in rats. *Toxicol Lett.* 2017;267:1–10.
- Nicholas DA, Proctor EA, Agrawal M, Belkina AC, Van Nostrand SC, Panneerseelan-Bharath L, et al. Fatty acid metabolites combine with reduced beta oxidation to

- activate Th17 inflammation in human type 2 diabetes. *Cell Metab.* 2019;30:447–61.e445.
24. Lee HK. Fatty acid overload to compromised oxidative phosphorylation activates inflammation in type 2 diabetes: hidden beasts and how to find them. *J Diabetes Investig.* 2020;11:290–3.
25. Freigang S, Ampenberger F, Weiss A, Kanneganti TD, Iwakura Y, Hersberger M, et al. Fatty acid-induced mitochondrial uncoupling elicits inflammasome-independent IL-1 α and sterile vascular inflammation in atherosclerosis. *Nat Immunol.* 2013;14:1045–53.
26. Hou Y, Wang Q, Han B, Chen Y, Qiao X, Wang L. CD36 promotes NLRP3 inflammasome activation via the mtROS pathway in renal tubular epithelial cells of diabetic kidneys. *Cell Death Dis.* 2021;12:523.
27. Ruan XZ, Varghese Z, Moorhead JF. An update on the lipid nephrotoxicity hypothesis. *Nat Rev Nephrol.* 2009;5:713–21.
28. Finucane OM, Lyons CL, Murphy AM, Reynolds CM, Klinger R, Healy NP, et al. Monounsaturated fatty acid-enriched high-fat diets impede adipose NLRP3 inflammasome-mediated IL-1 β secretion and insulin resistance despite obesity. *Diabetes.* 2015;64:2116–28.
29. Ralston JC, Lyons CL, Kennedy EB, Kirwan AM, Roche HM. Fatty acids and NLRP3 inflammasome-mediated inflammation in metabolic tissues. *Annu Rev Nutr.* 2017;37:77–102.
30. Swanson KV, Deng M, Ting JP. The NLRP3 inflammasome: molecular activation and regulation to therapeutics. *Nat Rev Immunol.* 2019;19:477–89.
31. Ruyschaert JM, Loney C. Role of lipid microdomains in TLR-mediated signalling. *Biochim Biophys Acta.* 2015;1848:1860–7.
32. O'Farrell M, Duke G, Crowley R, Buckley D, Martins EB, Bhattacharya D, et al. FASN inhibition targets multiple drivers of NASH by reducing steatosis, inflammation and fibrosis in preclinical models. *Sci Rep.* 2022;12:15661.
33. Liu X, Cooper DE, Cluntun AA, Warmoes MO, Zhao S, Reid MA, et al. Acetate production from glucose and coupling to mitochondrial metabolism in mammals. *Cell.* 2018;175:502–13.
34. Zhao S, Jang C, Liu J, Uehara K, Gilbert M, Izzo L, et al. Dietary fructose feeds hepatic lipogenesis via microbiota-derived acetate. *Nature.* 2020;579:586–91.
35. Lu J, Chen PP, Zhang JX, Li XQ, Wang GH, Yuan BY, et al. GPR43 deficiency protects against podocyte insulin resistance in diabetic nephropathy through the restoration of AMPK α activity. *Theranostics.* 2021;11:4728–42.

Springer Nature or its licensor (e.g. a society or other partner) holds exclusive rights to this article under a publishing agreement with the author(s) or other rightsholder(s); author self-archiving of the accepted manuscript version of this article is solely governed by the terms of such publishing agreement and applicable law.